Progress In Electromagnetics Research M, Vol. 95, 93–103, 2020

Slot-Type MIMO Antenna with Pattern and Circular Polarization Diversity for Mobile Applications

Sana Ullah and Zeeshan Zahid*

Abstract—Here we propose an L-shaped slot-type MIMO antenna with pattern and circular polarization diversity for WLAN applications. In order to maintain a low profile, the pattern and polarization diversities have been achieved without using additional supporting structures. Both the antenna elements are located at the corners of the same side of the ground plane. One of the antenna elements produces left hand circularly polarized (CP) waves whereas the other element produces right hand CP waves in (front) $+z$-direction. The senses of polarizations are opposite in (backward) $-z$-direction. CP waves have been generated using two orthogonal current modes, excited by locating the slots on the corner of the ground plane. The quadrature phase difference between the modes has been employed using the slot geometry. In other directions, the antenna correlation has been reduced using pattern diversity. The measured results confirm the simulated ones. The measured axial ratio bandwidth ($< 3\,\text{dB}$) and the matching bandwidth ($< -6\,\text{dB}$) are 380 MHz and 110 MHz, respectively. The envelop correlation coefficient is less than 0.1 in the operating band.

1. INTRODUCTION

High data rate communication is an ever increasing demand for modern mobile devices. Multiple input multiple output (MIMO) technology enhances channel capacity without additional bandwidth and power [1]. On the other hand, modern mobile devices are compact in sizes and possess high circuit density; therefore, the space limitation is critical for mobile device antennas. In order to meet the space limitation, the antennas need to be compact and closely spaced, which results in stronger mutual coupling. The coupling degrades the diversity performance [2] that can be controlled using a decoupling structure. Several decoupling structures have been proposed for reducing the mutual coupling between MIMO antennas of mobile devices, such as decoupling and matching networks [3, 4], electromagnetic band-gap structures [5], split ring resonators [6], neutralization lines [7], parasitic elements [8, 9], T-shaped slot, and defected ground structures [10]. The additional decoupling structure is an obstacle to maintain the low profile of the antenna system. In this regard, antenna isolation using pattern and polarization diversity is an interesting technique to achieve MIMO performance [11–14].

Circularly polarized (CP) antennas are attractive due to higher channel capacity, lower polarization loss factor, and less multipath interference [15] than linearly polarized antennas. However, higher channel capacity is not a unique feature of CP antennas as orthogonal linearly polarized antennas can also produce higher channel capacity [16]. The excitation techniques of circularly polarized antennas can be grouped into two main categories: dual orthogonal feed and single feed [17–19]. An additional power divider is required for dual orthogonal feed that adds to the complexity of the antenna structure. Therefore, single feed techniques are attractive due to low profile and ease of fabrication. For instance, L-shaped slot-type circularly polarized antennas were proposed for square shaped patch antennas

Received 27 April 2020, Accepted 7 July 2020, Scheduled 14 August 2020
* Corresponding author: Zeeshan Zahid (zeeshanzahid@mcs.edu.pk).
The authors are with the Department of Electrical Engineering, College of Signals, National University of Sciences and Technology, Rawalpindi 46000, Pakistan.

in [20, 21]. In the case of handheld device, it was established that the antenna used its chassis for efficient radiation [22]. Therefore, in order to generate circularly polarized waves, two orthogonal current modes of equal magnitude with quadrature phase difference need to be excited on the ground plane. In this regard, the theory of characteristic modes can be effectively utilized to design the CP antennas for mobile devices [23]. The characteristics of the ground modes can be controlled using a ground mode tuning (GMT) structures [24, 25]. The GMT consists of a metal strip attached at the periphery of the ground plane through an inductor. The structures were used to design CP antennas for mobile devices in various studies [26–28]. A CP antenna was proposed in [29] for arbitrary location on the ground plane where parasitic structures were used for phase compensation and magnitude regulation. The additional GMT and parasitic structures hinder the compactness of a mobile device. A few studies have reported CP antenna designs without additional structure. For instance, a loop-type ground radiation antenna was proposed for IoT devices without using the GMT structure in [30]. Furthermore, it is relatively simple to design a CP square shaped loop-type antenna without the ground plane [31]. CP chip antennas for GNSS applications were proposed in [32, 33] where the antenna structures were non co-planar.

A polarization diverse CP MIMO antenna was proposed for wearable devices using a GMT structure in [14]. In short, low profile CP diverse MIMO antennas with pattern diversity without additional decoupler or GMT structures for mobile devices still need more investigation. In this endeavour, we propose a low profile and easy to fabricate L-shaped slot-type MIMO antenna with circular polarization diversity for mobile devices without additional decoupler and GMT structures. The design mechanism of slot-type antennas is as follows.

The slot-type antenna excites loop-type currents around it in the ground plane, thereby acting as a magnetic coupler ($\overline{M}$). In general, the coupling (α) between the magnetic coupler and a characteristic ground mode ($\overline{J}$) can be expressed as [34]

$$\alpha = \frac{1}{1 + j\lambda} \iiint \overline{J} \cdot \overline{M} dv \tag{1}$$

where λ is the eigenvalue of the mode. Equation (1) indicates that the magnetic coupler exhibits maximum coupling with the ground mode when it is located at the maximum current of a ground mode. If the slot antenna is coupled with the first order mode ($\overline{J_1}$) of a rectangular ground plane of a mobile device, the horizontal current density on the ground plane becomes dominant. On the other hand, if the antenna is coupled with the second order mode ($\overline{J_2}$), the vertical current density on the ground plane becomes dominant. A mode is at resonance when its eigenvalue is zero. In order to excite the mode $\overline{J_1}$, the optimum location of the slot antenna is P_1 on the ground plane [33] where the coupling with $\overline{J_2}$ is minimal. Similarly, to excite $\overline{J_2}$, the optimum location of the antenna is P_2, exhibiting minimal coupling with $\overline{J_1}$. The antenna locations and the corresponding ground modes are depicted in Figure 1(a). Due to the dipole like current distributions of the modes, the antenna structure radiates linearly polarized waves. In order to excite both the modes using single antenna element, the slot needs to be located at the corner of the ground plane. At the corner, the electric coupling of the slot with both the modes must be enhanced because of higher magnitudes of modal electric fields. The coupling can be enhanced by the appropriate size of the slot. In terms of the electric coupling, the total current distribution ($\overline{J}_s$) on the ground plane can be expressed as follows [29]

$$\overline{J}_s = \frac{1}{1 + j\lambda_1} \left(\iiint \overline{J}_i \cdot \overline{E}_1 dv \right) \overline{J}_1 + \frac{1}{1 + j\lambda_2} \left(\iiint \overline{J}_i \cdot \overline{E}_2 dv \right) \overline{J}_2 \tag{2}$$

where λ_1 and λ_2 are the eigenvalues of the modes $\overline{J_1}$ and $\overline{J_2}$, respectively. The current density impressed by the antenna is $\overline{J}_i$ whereas $\overline{E}_1$ and $\overline{E}_2$ represent the electric fields radiated by the modes $\overline{J_1}$ and $\overline{J_2}$, respectively. Once both the modes are excited in phase, the total current distribution is diagonally excited, producing linearly polarized waves.

In order to generate circularly polarized waves, the modes $\overline{J_1}$ and $\overline{J_2}$ need to be excited on the ground plane with equal magnitude and quadrature phase shift. The conditions can be achieved using an L-shaped slot located near the corner of the ground plane with suitable excitation. The slot creates a microstrip line configuration oriented in horizontal and vertical directions, as shown in Figure 1(b) where the arrow indicates the location of the excitation. The length of the horizontal microstrip is

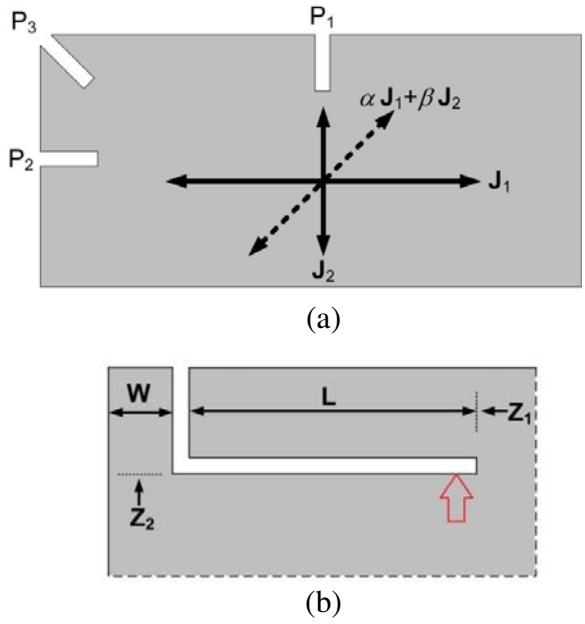

Figure 1. (a) The dominant current modes of a ground plane and (b) the L-shaped slot.

indicated by L whereas the width of the vertical microstrip is W. Parameter W also represents the location of the slot geometry with reference to the edge of the ground. The input impedances of the horizontal and vertical microstrip lines are represented by Z_1 and Z_2, respectively. The input impedance of an open circuit micro-strip line can be expressed as [35]

$$Z_{in} = R - jZ_o \cot(\beta l) \tag{3}$$

where Z_o is the characteristic impedance of the microstrip line, β the phase constant, and R the resistance due to conductor and dielectric loss. For an electrically small L-shaped slot, R is insignificant as compared to the imaginary part. Therefore, Z_1 and Z_2 are mainly capacitive which can be independently controlled using L and W, respectively. However, changing the length of the vertical microstrip simultaneously affects Z_1 and Z_2. The scheme can be extended to design polarization diverse MIMO antenna, as the slot geometry can be exploited to achieve right hand circularly polarized (RHCP) as well as left hand circularly polarized (LHCP) waves.

In this paper, we have demonstrated the MIMO design using pattern and CP diversity for a rectangular shaped wireless device, such as USB dongle, operating at 2.45 GHz WLAN band. The ground modes $\overline{J_1}$ and $\overline{J_2}$ of the rectangular ground plane resonate at different frequencies, offering different magnitudes of modal significances and arbitrary characteristic angles at the operating frequency. Therefore, achieving polarization diversity using CP conditions on the ground plane is a challenge.

2. ANTENNA DESIGN AND SIMULATION RESULTS

The geometry of the proposed CP MIMO antenna is displayed in Figure 2. The antenna has been designed on a 60 mm × 30 mm sized ground plane, a size of a typical USB dongle. FR4 material ($\varepsilon_r = 4.4$, $\tan\delta = 0.02$, thickness = 1.6 mm) has been used as a substrate. The antenna elements located at the upper and bottom corners are named as antenna 1 and antenna 2, respectively. Each antenna element consists of an L-shaped slot of width 0.5 mm etched at the corners of the same side of the ground plane. The geometries of both the antenna elements are flipped versions of each other. The length and width of the horizontal microstrip line are 9 mm and 3 mm, respectively, and those of vertical microstrip line are 3.5 mm and 1.5 mm, respectively. A coplanar waveguide of length 3 mm is used as a feeding structure that is attached with the horizontal strip through a lumped capacitor

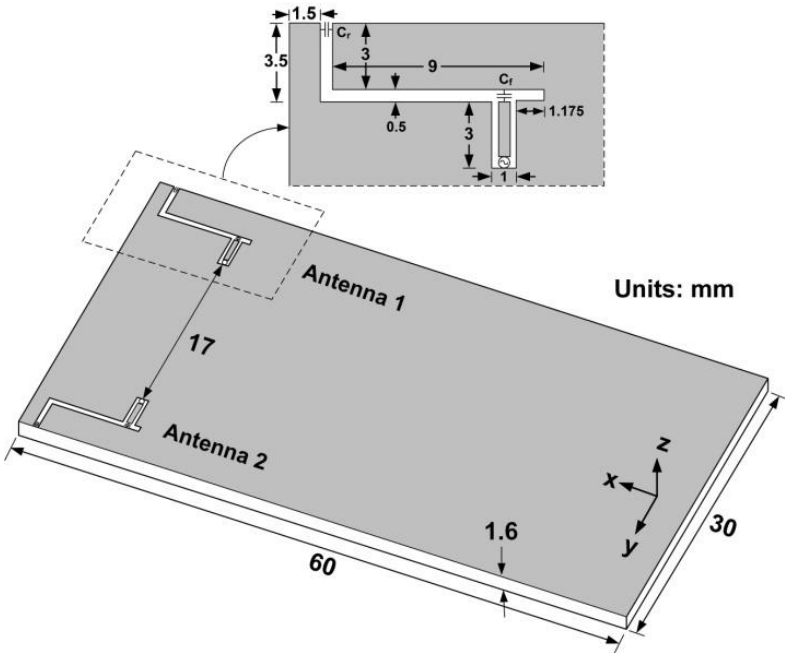

Figure 2. Geometry of the proposed antenna.

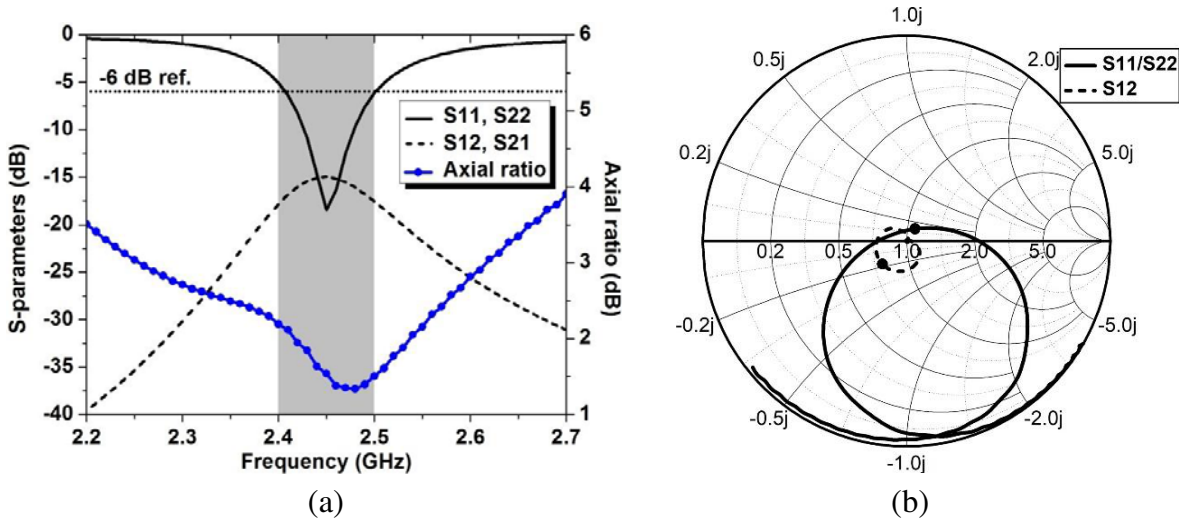

Figure 3. (a) Simulated S-parameters and axial ratio of the antenna. (b) Simulated S-parameters on Smith chart.

C_f. The operating frequency has been tuned using a resonance capacitor C_r whereas the impedance matching is controlled by the feeding capacitor C_f. Increasing the values of C_r lowers the operating frequency whereas the optimum value of C_f ensures impedance matching [36, 37].

The simulations were conducted in full-wave simulator HFSS to observe the antenna performance. The values of C_r and C_f used in the simulations were 0.23 pF and 0.5 pF, respectively. The simulation results of the proposed antenna are displayed in Figure 3. It can be observed in Figure 3(a) that the impedance bandwidth of the proposed antenna with reference to -6 dB is 95 MHz (2.41–2.50 GHz) which adequately covers the WLAN band. The maximum coupling (S_{12}) between the antennas is -14.96 dB at the operating frequency 2.45 GHz, which is acceptable for MIMO operation of mobile device antennas [38, 39]. The critical parameter characterizing circular polarization is axial ratio (AR).

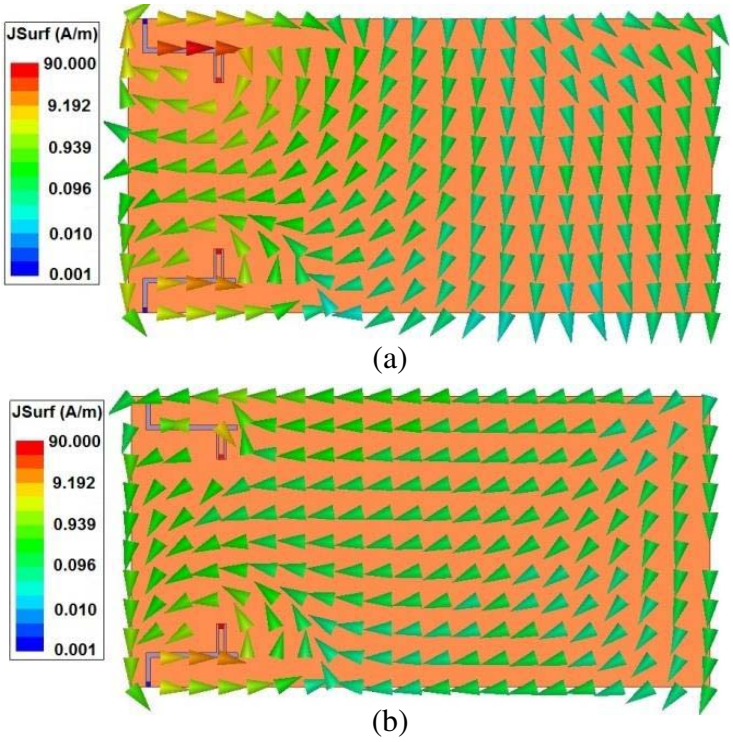

Figure 4. Simulated surface current distributions on the ground plane at (a) 0 degree phase, (b) 90 degree phase.

The simulated 3 dB AR bandwidth of the antenna in upward direction ($+z$-axis) is 370 MHz (2.25–2.62 GHz). Figure 3(b) shows the simulated S-parameters on the Smith chart from 1 GHz to 4 GHz. The figure indicates the coupling of the slot element with the ground plane as well as the coupling between the antenna elements. The feed structure rotates the reflection coefficient curve clockwise along the rim of the capacitive region of the Smith chart. The slot structure along with C_r bends the curve towards the centre of the Smith chart showing critical coupling with the ground plane. The S_{12} curve rotates close to the centre of the Smith chart indicating lower coupling between the antenna elements. The markers on the curves indicate the operating frequency.

The simulated surface current distributions at 2.45 GHz are illustrated in Figure 4 where antenna 1 was excited and antenna 2 terminated at the matched load. At zero degree phase, it can be observed that the surface current density is directed horizontally ($+x$-axis) whereas at 90° phase, the current density is directed vertically towards $+y$-axis. Therefore, the surface currents rotate in clockwise direction producing LHCP waves in the $+z$-axis. Similarly, when antenna 2 was excited, RHCP waves were generated along the $+z$-axis. The LHCP and RHCP radiation patterns are plotted in xz- and yz-planes in Figure 5 that confirm the polarization performance of the antenna.

Furthermore, the cross-polarization levels are below −20 dB along the z-axis. The phase difference between the horizontal and vertical components of the excited current density was controlled by the lengths of microstrip lines that, in turn, controlled the impedances Z_1 and Z_2. The calculated values of Z_1 and Z_2 at the operating frequency were 1.127–29.8j Ω and 3–146.5j Ω, respectively. Due to the higher capacitive reactance of Z_2 than Z_1, the horizontal component of the excited current density leads the vertical component by 90°. As a result, the antenna produced LHCP waves in the $+z$-axis and RHCP waves in $-z$-axis. Simulations further revealed that the real parts of Z_1 and Z_2 did not change significantly with frequency whereas the corresponding imaginary parts increased gradually. Therefore, the phase difference between the horizontal and vertical components of the excited current density remained close to 90° for a wider frequency range, resulting in wider AR bandwidth.

Simulations were conducted to observe the effects of lengths L and W on AR, and the results of the parametric analysis are presented in Figure 6. It can be observed that the increases in L and W shift

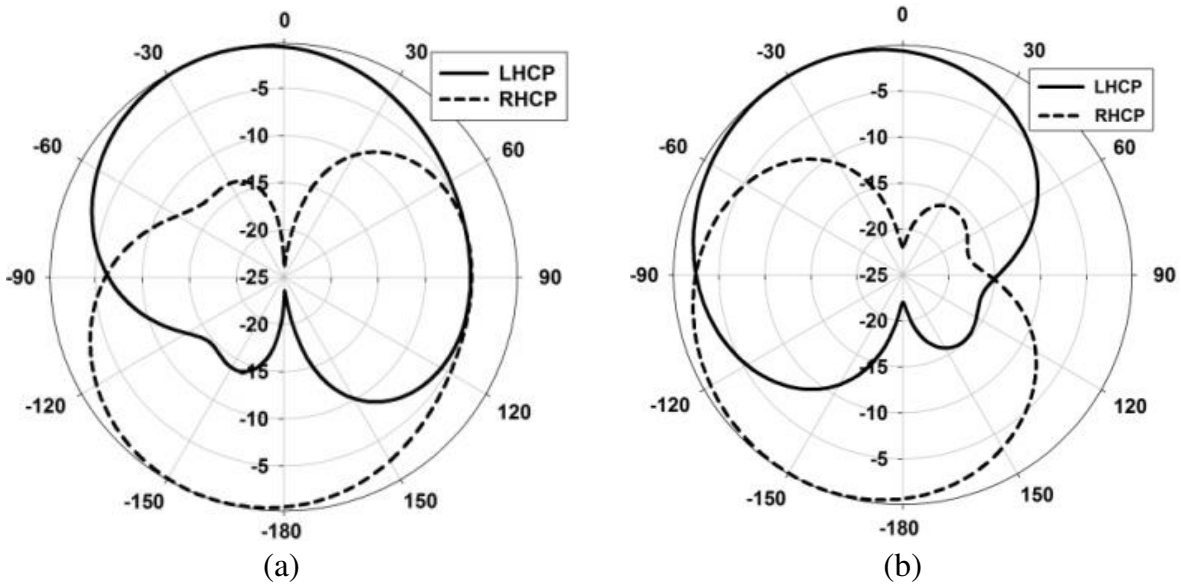

Figure 5. The simulated LHCP and RHCP radiation patterns at 2.45 GHz in the (a) xz-plane, (b) yz-plane.

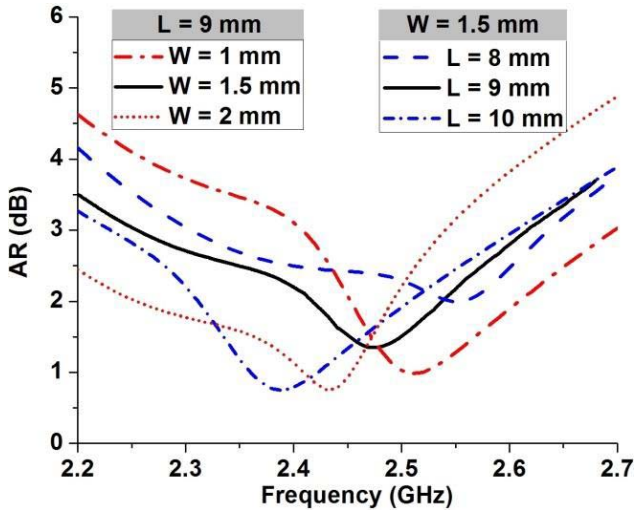

Figure 6. Parametric analysis of axial ratio with the slot length and location on the ground plane.

the AR curves toward the lower frequencies. Moreover, increasing L lowers the operating frequency of the antenna that can be adjusted using C_r. However, changing the values of C_r and C_f does not significantly affect the AR, which is the key to the tuning mechanism of the antenna. Figure 6 also reveals that the slot geometry can be modified to generate elliptically polarized waves whereas shifting the L-shaped slot towards position P_2 on the ground plane generates linearly polarized waves. The simulated 3D gain patterns of each antenna element when the other antenna was terminated at the matched load are plotted in Figure 7. The figure shows that the value of the peak gain is 1.2 dB that lies in xy-plane ($\theta = 90°$). The peak gain of antenna 1 is at $\phi = 240°$ whereas that of antenna 2 is at $\phi = 120°$. The gain at the z-axis is -1.4 dB. Furthermore, the gain pattern of antenna 1 has a -15 dB null towards the $+y$-axis whereas that of antenna 2 is along the $-y$-axis. The observations demonstrate the pattern diversity of the MIMO antenna.

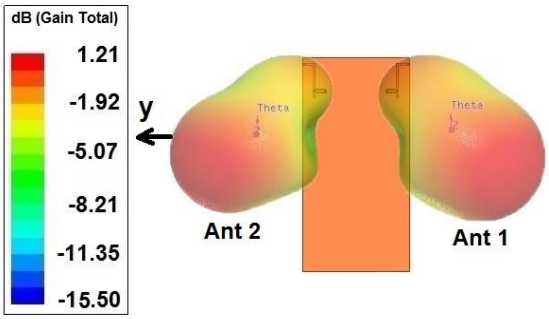

Figure 7. Gain pattern diversity of the proposed MIMO antenna.

Figure 8. Fabricated antenna.

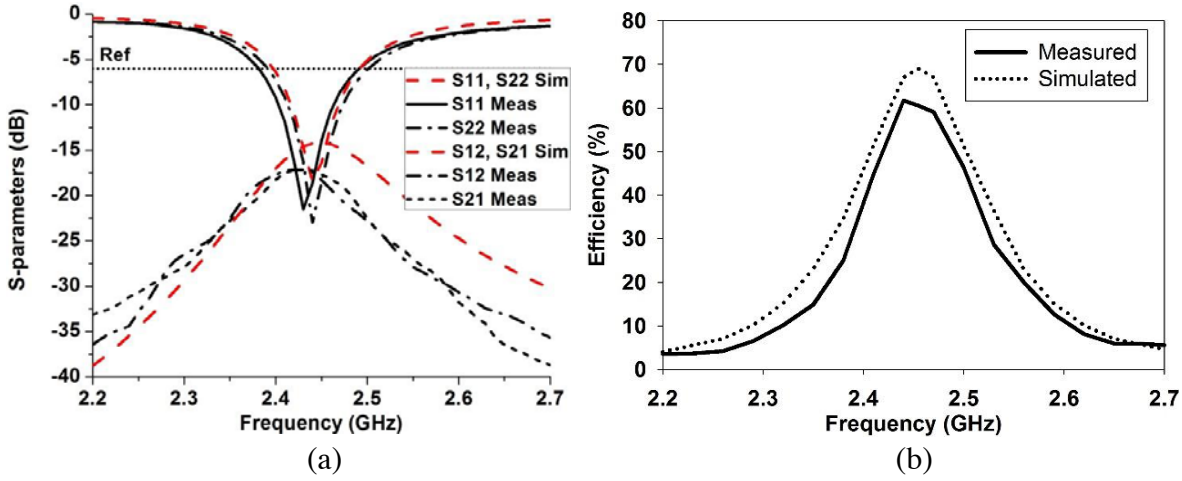

Figure 9. Simulated and measured (a) S-parameters, (b) total efficiency.

3. MEASURED RESULTS AND DISCUSSION

Experiments were conducted to validate the performance of the proposed design. The snapshot of the fabricated antenna is displayed in Figure 8. The values of fabricated C_r and C_f were 0.2 pF and 0.4 pF, respectively. The S-parameters were measured using Agilent's E8362 network analyzer. Figure 9(a) compares the simulated and measured S-parameters. The measured bandwidth of both antennas with reference to -6 dB was 110 MHz, antenna 1 (2.38–2.49 GHz) and antenna 2 (2.39–2.5 GHz). The maximum coupling between the antenna elements was -17.18 dB. Figure 9(b) shows the simulated and measured efficiencies of the antenna element. It can be observed that the peak value of the efficiency occurs at the operating frequency where the peak value of the measured total efficiency is 62%. The envelope correlation coefficient (ECC) was calculated using the measured radiation patterns as

$$\mathrm{ECC} = \frac{\left| \iint\limits_{4\pi} G_1(\theta,\phi) G_2(\theta,\phi) d\Omega \right|^2}{\iint\limits_{4\pi} |G_1(\theta,\phi)|^2 \, d\Omega \iint\limits_{4\pi} |G_2(\theta,\phi)|^2 \, d\Omega} \tag{4}$$

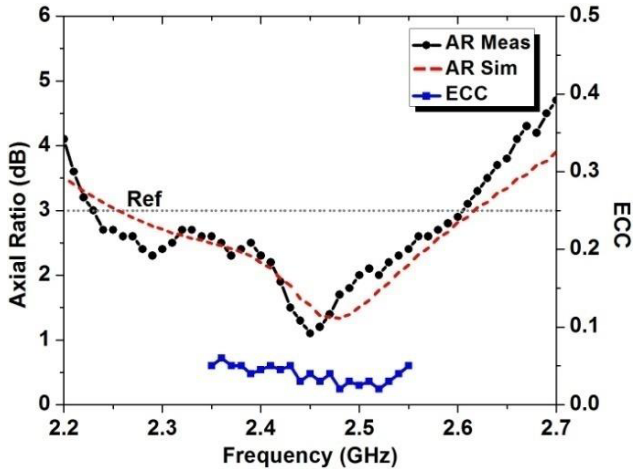

Figure 10. Measured axial ratio and ECC of the antenna.

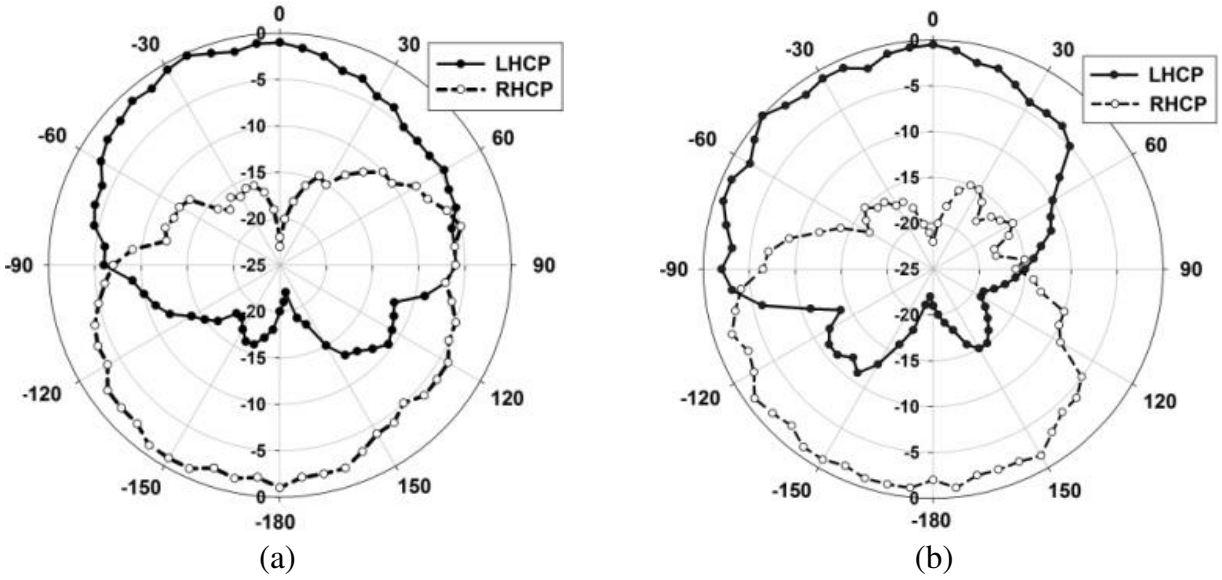

Figure 11. Polarization patterns in (a) xz-plane, (b) yz-plane.

where $G_i(\theta, \phi)$ is the radiation pattern of the MIMO antenna when port i is excited [40]. Figure 10 depicts the measured AR and ECC. The figure shows that the measured AR bandwidth is 380 MHz that stretches from 2.23 GHz to 2.61 GHz, where the minimum value of AR is 1.1 dB at 2.44 GHz. The ECC was measured from 2.35 GHz to 2.55 GHz where it can be noted that the ECC values are well below 0.5. The radiation patterns were measured in an anechoic chamber of size $9 \times 5 \times 5\,\text{m}^3$. The measured polarization patterns are displayed in Figure 11. It can be observed that the antenna produced LCHP waves in $+z$-axis and RHCP waves in $-z$-axis. The measured cross polarization levels were below -18 dB, demonstrating polarization diversity. The measured total gain patterns in xy, xz, and yz-planes are plotted in Figure 12 when antenna 1 was excited. The measured peak gain was 1.1 dB whereas the gain in the direction of antenna 2 ($+y$-axis) was -17 dB. The experimental results demonstrate that the proposed antenna, maintaining low profile, achieved satisfactory CP diversity performance.

The performance of the proposed MIMO antenna is compared with those of existing literature in Table 1. It can be seen that the AR bandwidth of the proposed antenna is better than all the references presented in the table except that of [12]. The AR bandwidth achieved in [12] is mainly attributed to larger ground size and additional T-shaped structure. However, the matching bandwidths of [14, 26–28]

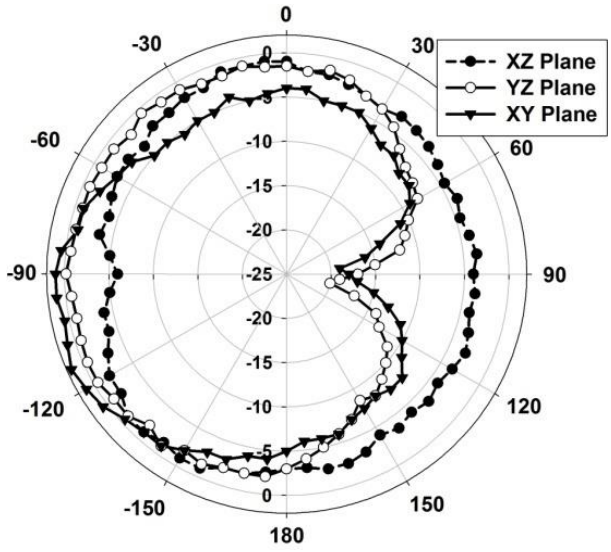

Figure 12. Measured radiation pattern at 2.45 GHz.

Table 1. Comparison of proposed design with literature.

Ref.	PCB Size (mm^2)	3 dB ARBW (MHz)	−6 dB Matching BW (MHz)	Centre Freq. (GHz)	Supporting structure	MIMO performance (ECC)
[12]	68×68	660	750	1.45	Protruding ground	< 0.02
[14]	30×30	> 100	170	2.45	GMT	< 0.1
[26]	30×30	140	170	2.45	GMT	N.A
[27]	45×45	130	150	2.45	GMT	N.A
[28]	30×30	260	180	2.45	2 GMTs	N.A
[29]	140×70	120	80	1.57	Phase compensator	N.A
[30]	60×30	300	110	2.45	Nil	N.A
Prop.	60×30	380	110	2.45	Nil	< 0.05

are higher than the proposed antenna, mainly because of the additional GMT structure. Furthermore, the MIMO performance of the proposed antenna is better than that of [14]. The proposed design demonstrates good axial ratio bandwidth compared to the embedded mobile devices antennas of the literature; however, the matching bandwidth is lower than those of many articles. The bandwidth can be enhanced by enhancing the coupling between the slot and the ground plane. One of the methods is to use a series resonator circuit in the feeding strip. The impedance level ($\sqrt{L/C}$) can be used to improve the coupling [41]. Furthermore, increasing the slot area can also enhance the matching bandwidth.

4. CONCLUSION

We proposed an L-shaped slot-type MIMO antenna with pattern and circularly polarization diversity for WLAN applications. The CP conditions were achieved using the slot location and its geometry. Both the antenna elements generated opposite sense circularly polarized waves along the z-axis, exhibiting pattern diversity, without additional supporting structures. The measured matching and AR bandwidths were 110 MHz and 380 MHz, respectively. The cross polarization levels and ECC were below −18 dB and 0.1, respectively. The design scheme can be utilized in wireless IoT devices.

REFERENCES

1. Foschini, G. J. and M. J. Gans, "On limits of wireless communication in a fading environment when using multiple antennas," *Wireless Personal Commun.*, Vol. 6, 311–335, 1998.
2. Chen, X., S. Zhang, and Q. Li, "A review of mutual coupling in MIMO systems," *IEEE Access*, Vol. 6, 24706–24719, 2018.
3. Chen, S. C., Y. S. Wang, and S. J. Chung, "A decoupling technique for increasing the port isolation between two strongly coupled antennas," *IEEE Trans. Antennas Propag.*, Vol. 6, No. 12, 3650–3658, 2008.
4. Tang, X., K. Mouthaan, and J. C. Coetzee, "Tunable decoupling and matching network for diversity enhancement of closely spaced antennas," *IEEE Antennas and Wireless Propagation Letters*, Vol. 11, 268–271, 2012.
5. Lee, J. Y., S. H. Kim, and J.-H. Jang, "Reduction of mutual coupling in planar multiple antenna by using 1-D EBG and SRR structures," *IEEE Trans. Antennas Propag.*, Vol. 63, No. 9, 4194–4198, 2015.
6. Ramachandaran, A., S. V. Pushpakaran, M. Pezholil, et al., "A four-port MIMO antenna using concentric square-ring patches loaded with CSRR for high isolation," *IEEE Antennas and Wireless Propagation Letters*, Vol. 15, 1196–1199, 2016.
7. Su, S. W., C. T. Lee, and F. S. Chang, "Printed MIMO-antenna system using neutralization-line technique for wireless USB-dongle applications," *IEEE Trans. Antennas Propag.*, Vol. 60, No. 9, 456–463, 2012.
8. Zahid, M. Z., L. Qu, H. H. Kim, and H. Kim, "Decoupler design for MIMO antennas of USB dongle applications using ground mode coupling analysis," *Progress In Electromagnetic Research M*, Vol. 76, 113–122, 2018.
9. Qu, L., R. Zhang, and H. Kim, "Decoupling between ground radiation antennas with ground coupled loop-type isolator for WLAN applications," *IET Microw. Antennas and Propag.*, Vol. 10, No. 5, 546–552, 2016.
10. Luo, C. M., J. S. Hong, and L. L. Zhong, "Isolation enhancement of a very compact UWB-MIMO slot antenna with two defected ground structures," *IEEE Antennas and Wireless Propagation Letters*, Vol. 14, 1766–1769, 2015.
11. Kharche, S., G. S. Reddy, R. K. Gupta, and J. Mukherjee, "Wide band circularly polarised diversity antenna for satellite and mobile communication," *IET Microw. Antennas and Propag.*, Vol. 11, No. 13, 1863–1869, 2017.
12. Yao, Y., X. Wang, X. Chen, et al., "Novel diversity/MIMO PIFA antenna with broadband circular polarization for multimode satellite navigation," *IEEE Antennas and Wireless Propagation Letters*, Vol. 11, 65–68, 2012.
13. Dietrich, C. B., K. Dietze, J. R. Nealy, and W. L. Stutzman, "Spatial, polarization, and pattern diversity for wireless handheld terminals," *IEEE Trans. Antennas Propag.*, Vol. 49, No. 9, 1271–1281, 2001.
14. Qu, L., H. Piao, Y. Qu, et al., "Circularly polarised MIMO ground radiation antennas for wearable devices," *Electron. Lett.*, Vol. 54, No. 4, 189–190, 2018.
15. Dicandia, F. A., S. Genovesi, and A. Monorchio, "Analysis of the performance enhancement of MIMO systems employing circular polarization," *IEEE Trans. Antennas Propag.*, Vol. 65, No. 9, 4824–4835, 2017.
16. Grau, A., J. Romeu, M. Lee, et al., "A dual-linearly-polarized MEMS-reconfigurable antenna for narrowband MIMO communication systems," *IEEE Trans. Antennas Propag.*, Vol. 58, No. 1, 4–17, 2010.
17. Balanis, C. A., *Antenna Theory: Analysis and Design*, 4th Edition, Wiley Inter-Science, Hoboken, NJ, USA, ISBN: 978-1-119-17899-6, 2016.
18. Gao, S. S., Q. Luo, and F. Zhu, *Circularly Polarised Antennas*, Wiley, Hoboken, NJ, USA, 2014.
19. Garg, R., P. Bhartia, I. Bahl, et al., *Microstrip Antenna Design Handbook*, Artech House, 2001.

20. Mousavi, P., B. Miners, and O. Basir, "Wideband L-shaped circularly polarised monopole slot antenna," *IEEE Antennas and Wireless Propagation Letters*, Vol. 9, 822–825, 2010.
21. Yang, S., A. Kishk, and K. Lee, "Wideband circularly polarised antenna with L-shaped slot," *IEEE Trans. Antennas Propag.*, Vol. 56, No. 6, 1780–1783, 2008.
22. Vainikainen, P., J. Ollikainen, O. Kivekas, et al., "Resonator based analysis of the combination of mobile handset antenna and chassis," *IEEE Trans. Antennas Propag.*, Vol. 50, No. 10, 1433–1444, 2002.
23. Fabres, M. C., E. Antonio, A. V. Nogueira, et al., "The theory of characteristic modes revisited: A contribution to the design of antennas for modern applications," *IEEE Antennas and Propag. Magazine*, Vol. 49, No. 5, 52–68, 2007.
24. Qu, L., R. Zhang, H. Shin, J. Kim, et al., "Performance enhancement of ground radiation antenna for Z-wave applications using tunable metal loads," *Electron. Lett.*, Vol. 52, 1827–1828, 2016.
25. Zahid, Z. and H. Kim, "Enhancement technique for loop type ground radiation antenna using ground mode tuning structure," *Microwave and Optical Technology Lett.*, Vol. 59, No. 1, 476–478, 2017.
26. Qu, L., Z. Zahid, H.-H. Kim, and H. Kim, "Circular polarised ground radiation antenna for mobile applications," *IEEE Trans. Antennas Propag.*, Vol. 66, No. 5, 2655–2660, 2018.
27. Zahid, Z., L. Qu, H.-H. Kim, et al., "Circularly polarised loop-type ground radiation antenna for IoT applications," *Journal of Electromagnetic Engineering and Science*, Vol. 19, No. 2, 153–158, 2019.
28. Park, D., L. Qu, and H. Kim, "Compact circularly polarised antenna utilising the radiation of the ground plane based on the theory of characteristic modes," *IET Microw. Antennas and Propag.*, Vol. 13, No. 10, 1509–1514, 2019.
29. Qu, L. and H. Kim, "A novel single-feed dual-element antenna using phase compensation and magnitude regulation to achieve circular polarization," *IEEE Trans. Antennas Propag.*, Vol. 66, No. 10, 5098–5108, 2018.
30. Zahid, Z., L. Qu, H.-H. Kim, et al., "Circularly polarised loop-type ground radiation antenna for mobile devices using a resonance inductor and capacitor," *Electron. Lett.*, Vol. 54, No. 5, 262–264, 2018.
31. Lei, W., H. Chu, and Y.-X. Guo, "Design of a circularly polarised ground radiation antenna for biomedical applications," *IEEE Trans. Antennas Propag.*, Vol. 64, No. 6, 2535–2540, 2016.
32. Chang, S. H. and W. J. Liao, "A novel dual band circularly polarised GNSS antenna for handheld devices," *IEEE Trans. Antennas Propag.*, Vol. 61, No. 1, 555–562, 2013.
33. Liao, W.-J., J.-T. Yeh, and S.-H. Chang, "Circularly polarised chip antenna design for GPS reception on handsets," *IEEE Trans. Antennas Propag.*, Vol. 62, No. 7, 3482–3489, 2014.
34. Harrington, R. F., *Time-harmonic Electromagnetic Fields*, Wiley-Interscience, New York, NY, USA, 2001.
35. Pozar, D. M., *Microwave Engineering*, 4th Edition, Wiley, ISBN 978-0-470-63155-3, 2011.
36. Liu, Y., J. Lee, H. H. Kim, and H. Kim, "Ground radiation using slot with coupling capacitor," *Electron. Lett.*, Vol. 49, No. 7, 447–448, 2013.
37. Zahid, Z. and H. Kim, "Analysis of a loop type ground radiation antenna based on equivalent circuit model," *IET Microw. Antennas and Propag.*, Vol. 11, No. 1, 23–28, 2016.
38. Liu, D. Q., M. Zhang, H. J. Luo, et al., "Dual-band platform-free PIFA for 5G MIMO application of mobile devices," *IEEE Trans. Antennas Propag.*, Vol. 66, No. 11, 6328–6333, 2018.
39. Soltani, S. and R. D. Murch, "A compact planar printed MIMO antenna design," *IEEE Trans. Antennas Propag.*, Vol. 63, No. 2, 1140–1149, 2015.
40. Vaughan, R. G. and J. B. Andersen, "Antenna diversity in mobile communications," *IEEE Trans. Veh. Technol.*, Vol. 36, No. 4, 149–172, 1987.
41. Zhang, R., Y. Liu, H. H. Kim, et al., "Bandwidth enhancement of ground antenna using resonant feeding circuit," *Electron. Lett.*, Vol. 49, 441–442, 2013.